npj | 2D materials and applications

www.nature.com/npj2dmaterials

ARTICLE OPEN

Check for updates

Ultrafast hot carrier transfer in WS_2/graphene large area heterostructures

Chiara Trovatello[1], Giulia Piccinini[2,3], Stiven Forti[2], Filippo Fabbri[2,4,6], Antonio Rossi[2,3,7,8], Sandro De Silvestri[1,5], Camilla Coletti[2,4], Giulio Cerullo[1,5] and Stefano Dal Conte[1]✉

Charge transfer processes in two-dimensional van der Waals heterostructures enable upconversion of low energy photons and efficient charge carriers extraction. Here we use broadband ultrafast optical spectroscopy to track charge transfer dynamics in large-area 2D heterostructures made of epitaxial single-layer tungsten disulfide (WS_2) grown by chemical vapour deposition on graphene. Selective carrier photoexcitation in graphene, with tunable near-infrared photon energies as low as 0.8 eV (i.e. lower than half of the optical bandgap of WS_2), results in an almost instantaneous bleaching of the WS_2 excitonic peaks in the visible range, due to the interlayer charge transfer process. We find that the charge transfer signal is strongly non-linear with the pump fluence and it becomes progressively more linear at increasing pump photon energies, while the interlayer photoinjection rate is constant in energy, reflecting the spectrally flat absorbance of graphene. We ascribe the interlayer charge transfer to a fast transfer of hot carriers, photogenerated in graphene, to the semiconducting layer. The measured sub-20-fs hot-carrier transfer sets the ultimate timescale for this process. Besides their fundamental interest, our results are technologically relevant because, given the capability of large-area deterministic growth of the heterostructure, they open up promising paths for novel 2D photodetectors, also potentially scalable to industrial platforms.

npj 2D Materials and Applications (2022)6:24 ; https://doi.org/10.1038/s41699-022-00299-4

INTRODUCTION

When carriers in a semiconductor are excited by an ultrashort laser pulse they can gain, due to multiple carrier-carrier scattering events, excess energy that is much higher than the characteristic energy associated with the thermal fluctuations, and rise well above the Fermi energy. Such high-energy carriers are denoted as hot carriers. Hot carriers have always played a central role in semiconductors from the point of view of both fundamental physics and device engineering[1–3]. Hot-carrier injection processes have been reported to increase the conversion efficiency of solar cells[4]. Photodetectors based on hot-carrier injection through a metal-semiconductor Schottky junction or a metal-oxide tunneling barrier enable photovoltaic energy conversion at energies below the semiconductor gap[5,6]. Efficient photoinjection of hot carriers in semiconductors is observed at early times following photoexcitation. This process creates a non-equilibrium distribution of electrons (holes) above (below) the Fermi energy with excess kinetic energy. The electron-electron scattering process occurs usually during the first tens of femtoseconds and creates a Fermi-Dirac distribution, corresponding to a high electronic temperature T_e, with a tail extending to high energies[7,8]. The excess energy stored by the electronic bath is rapidly converted to heat because of the scattering with phonons on a (sub)-picosecond timescale, resulting in equilibrated electronic (T_e) and lattice (T_l) temperatures.

Thanks to its unique electronic and optical properties, graphene has emerged as a very promising material for a new generation of photonic and optoelectronic devices[9], such as optical modulators[10,11], fast photodetectors[12,13] and plasmonic devices[14,15]. In graphene, the build-up of the hot carriers distribution and the subsequent relaxation processes are strongly influenced by the peculiar linear dispersion of the Dirac bands and by the kinematic constraints imposed by two-dimensional confinement. Electron-electron scattering processes, such as intra- and inter-band scattering, carrier multiplication and Auger recombination, lead to the extremely rapid generation (i.e. over a few tens of femtoseconds) of a hot-carrier population which is characterized by an energy and a temperature higher than respectively the Fermi level and the temperature of the phonon bath[7,16–20]. Even at moderate excitation fluences, due to the low electronic heat capacitance[21], comparatively high temperatures of the order of 1000 K can be reached. On a longer timescale (i.e. few ps) different relaxation channels, such as scattering with optical and acoustic phonons, determine the cooling process of the hot carriers.

Due to its 2D nature, graphene offers unique advantages for manipulating hot carriers in nanoscale devices. Recently van der Waals heterostructures (HS), obtained by stacking graphene sheets with other 2D crystals (e.g. boron nitride, transition metal dichalcogenides or graphene itself), have received remarkable attention because they offer the possibility to realize atomically thin optoelectronic devices with tailored optical properties.

Transition metal dichalcogenides (TMDs) are layered semiconductors consisting of crystalline sheets with strong intralayer covalent bonds and weak interlayer van der Waals interactions. When thinned down to a single-layer (1L), they exhibit a direct bandgap and strong light-matter interactions, with the optical spectra dominated by excitons with large binding energies (hundreds of meV). Graphene/TMD HSs have the advantage to

[1]Dipartimento di Fisica, Politecnico di Milano, Piazza Leonardo da Vinci 32, I-20133 Milano, Italy. [2]Center for Nanotechnology Innovation @ NEST, Istituto Italiano di Tecnologia, Piazza San Silvestro 12, 56127 Pisa, Italy. [3]NEST, Scuola Normale Superiore, P.zza San Silvestro 12, 56127 Pisa, Italy. [4]Graphene Labs, Via Morego 30, 16163 Genova, Italy. [5]IFN-CNR, Piazza L. da Vinci 32, I-20133 Milano, Italy. [6]Present address: NEST, Istituto Nanoscienze-CNR, Piazza San Silvestro 12, 56127 Pisa, Italy. [7]Present address: Department of Physics, University of California, Davis, CA 95616, USA. [8]Present address: Advanced Light Source, Lawrence Berkeley National Laboratory, Berkeley, CA 94720, USA. ✉email: stefano.dalconte@polimi.it

combine the strong light-matter interaction of TMDs, enhanced by the excitonic effects, with the broadband absorption and the high carrier mobility of graphene[22–24]. For this reason, photodetectors based on these HSs display a high responsivity and a fast (i.e. few ps) photoresponse[24,25]. Despite the high optoelectronic performance of such devices, the non-equilibrium optical response and in particular the interlayer charge carrier dynamics in graphene/TMD HS are still objects of controversy. In particular, the origin of the interlayer charge transfer (CT) from graphene to the TMD upon selective photoexcitation below the bandgap of the semiconductor is still not clear. Experimental evidence suggested two alternative explanations for the CT process: (i) direct excitations of CT states from the valence band of graphene to the conduction band of the TMD[26]; (ii) photothermionic emission[27,28]. The latter mechanism involves two sequential steps: the formation of a hot-electron (and hole) distribution in graphene upon photoexcitation on a 10 fs timescale[7] and the subsequent interlayer transfer to the TMD. In the transfer process only a small fraction of photoexcited carriers—i.e. those in the high-energy tail of the distribution—have sufficient energy to overcome the Schottky barrier ϕ of the graphene/TMD heterojunction[27–29].

Recent experiments have shown that the photocurrent in a graphene/few-layer TMD HS device scales non-linearly with the fluence for photoexcitation below the bandgap of the TMD, strongly supporting the photothermionic mechanism[27,30]. Conversely, transient absorption measurements performed on graphene/1L-WS_2 HS reported a linear scaling of the WS_2 excitonic bleaching signal with the pump incident fluence[26]—supporting a direct excitation process. On the other hand, Chen et al.[28] suggest that the linear power dependence is the result of fast interlayer scattering of hot electrons and holes before the electron-hole thermalization and propose a model that goes beyond the usual one based on photothermionic emission, where two different chemical potentials are assigned to electrons and holes. However, this model is not able to capture the non-linear power dependence of excitonic bleaching and its evolution to the linear regime for increasing pump photon energies (as we will show later). Since a general agreement on the scattering mechanism governing the photophysics of graphene-TMD HS is still not reached, further ultrafast studies are needed to better understand the interlayer CT process. In particular, high temporal resolution is strongly beneficial for resolving the formation process of the hot-carrier distribution in graphene and the transfer process through the HS interface.

Here we perform ultrafast transient reflectivity spectroscopy, combining sub-20-fs temporal resolution with broad spectral coverage, to investigate the charge transfer dynamics in a large-area 1L-WS_2/graphene HS. We find that excitation below the WS_2 bandgap, at a technologically relevant telecom wavelength (i.e. 1550 nm–0.8 eV), results in the prompt formation of the transient excitonic signal in the TMD, which super-linearly increases with the pump fluence. We ascribe this result to a fast scattering of hot carriers which are selectively photogenerated in the graphene layer and, even before the electron-electron thermalization is fully accomplished, are injected into the TMD layer. By directly comparing the build-up of the hot-carrier distribution in graphene and the WS_2 A excitonic resonance, we estimate 20 fs as the upper limit of the CT process. We also find that, at higher pump photon energies, the excitonic transient signal progressively changes the power-law scaling, displaying a linear power dependence for above-bandgap excitation. Interestingly, the transient excitonic signal displays hundreds of ps lifetime. This observation is promising in view of the development of high responsivity graphene/TMD photodetectors excited below the bandgap of the semiconductor. Our results provide fundamental insights into the physical mechanisms which determine the efficiency of graphene/TMD-based optoelectronic devices, and open up promising paths for new 2D optoelectronic devices towards large-scale production.

RESULTS AND DISCUSSION

Large-area WS_2/graphene heterostructures

The large-area WS_2/graphene HS sample consists of a single-crystal chemical vapour deposition (CVD) grown graphene and an epitaxial 1L-WS_2, also grown by CVD, as shown in the schematic (Fig. 1a). Graphene, first grown on a copper foil and subsequently transfered onto the SiO_2/Si substrate, has lateral dimensions of hundreds of μm (see Fig. 1b). WS_2 is then CVD grown on top of graphene/SiO_2/Si (Fig. 1c). Unlike HSs obtained by mechanical exfoliation with a lateral size of a few tens of microns, our graphene sample has a lateral size of ~400 μm and its deterministic growth by CVD in large arrays has the advantage of large-area scalability and potential extension to wafer-scale processing[31]. Moreover, 1L-WS_2 preferentially grows azimuthally aligned with the underlying graphene flake[32–34].

Broadband transient reflectivity of WS_2/graphene heterostructures

We perform broadband transient reflectivity ($\Delta R/R$) experiments to measure the non-equilibrium dynamics of the HS, using the experimental setup sketched in Supplementary Fig. 9. Since the HS is on a reflective SiO_2/Si substrate, the $\Delta R/R$ signal is effectively equivalent to a double-pass differential transmission measurement. We use frequency tunable ultrashort laser pulses, obtained by a non-collinear optical parametric amplifier (NOPA), to photoexcite the sample respectively above and below the optical gap of the WS_2 (i.e. 1.98 eV). The probe pulse is a white light continuum with a broad spectral content (1.7–2.6 eV) covering both A and B excitonic resonances of WS_2. Pump and probe beams have diameters of ~230 μm and ~150 μm, respectively, smaller than the ~400 μm lateral dimension of the heterostructure, to ensure uniform excitation and detection on the sample. The temporal relaxation of photoexcited carriers/excitons is measured by acquiring the differential reflectivity map $\Delta R/R(E_{probe}, \tau)$, as a function of the pump-probe delay τ and the probe photon energy E_{probe}. All the measurements are performed at room temperature, under ambient conditions.

The differential reflectivity map measured on WS_2/graphene HS with photoexcitation above the semiconductor gap, reported in Fig. 2a, is very similar to that of 1L-WS_2 alone (see Supplementary Fig. 4). Here the pump photon energy is tuned on resonance with the A exciton peak (i.e. 1.98 eV). Although at this photon energy both graphene and 1L-WS_2 are excited, the $\Delta R/R$ spectrum is dominated by the A/B excitonic features of 1L-WS_2. As a matter of fact, the strong excitonic effects significantly enhance the light absorption, which in 1L-WS_2 is ~10%[35] around the A exciton peak, i.e. more than a factor of 5 higher than the ~2% absorbance of graphene[36].

The positive $\Delta R/R$ signals centred, respectively at ~1.98 eV and ~2.4 eV are mainly ascribed to the pump-induced bleaching of the excitonic transitions due to the phase-space filling effect, i.e. the so-called Pauli-blocking mechanism. Additional many-body effects, leading to a transient renormalization of the exciton binding energy and the electronic bandgap, also play an important role[37]. A clear signature of the interplay between Pauli-blocking and many-body effects is a transient blue-shift (~50 meV) of the maximum of the positive $\Delta R/R$ signal occurring within the first few ps. The same shift has been observed in 1L-WS_2 and previously in other TMDs[37–40]. The relaxation dynamics measured on the HS and 1L-WS_2 alone display the same behaviour (see Supplementary Fig. 6) and are characterized by a rapid decay followed by a long-lived component with tens-to-hundreds of ps lifetime. These results differ from previous transient optical measurements on mechanically exfoliated graphene-TMD HSs, which have shown a drastic reduction of the decay time constant with respect to the isolated TMD[26,41,42]. The observed change of the relaxation dynamics has been

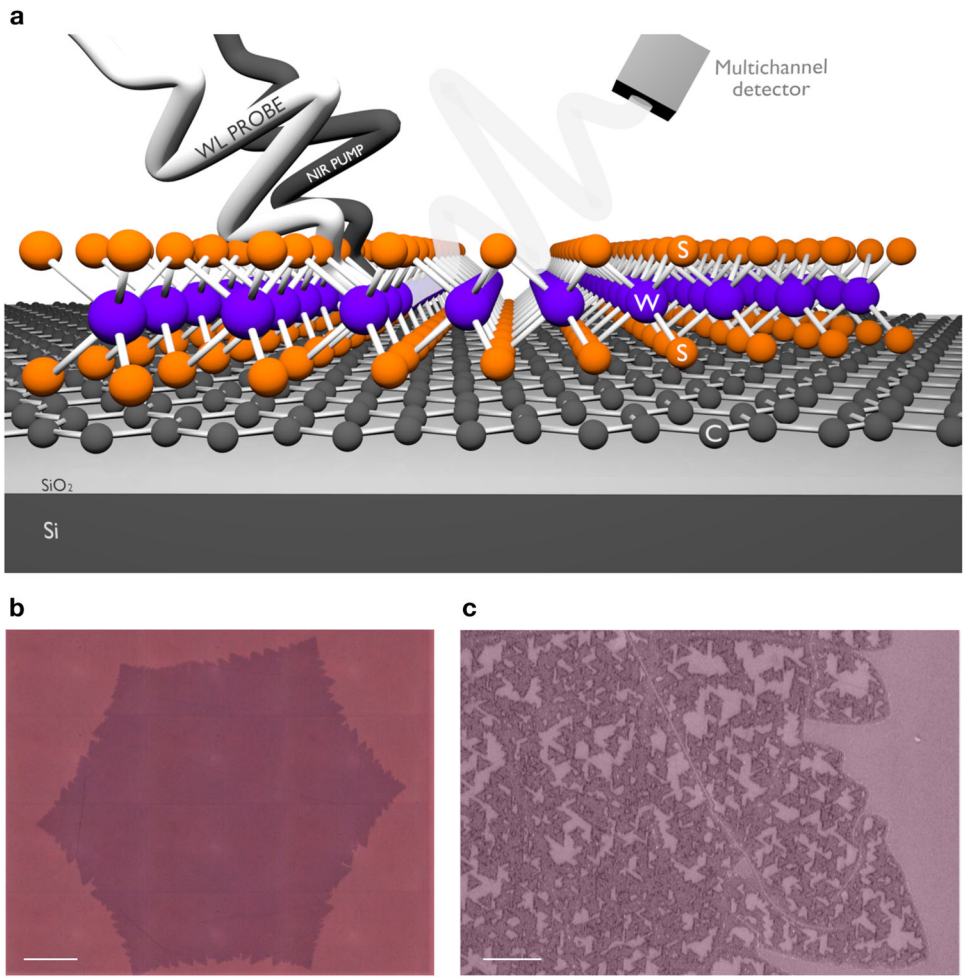

Fig. 1 Sample structure. a Schematic of the WS_2/graphene heterostructure on SiO_2/Si substrate photoexcited by an ultrashort near-IR pulse. The white light probe is reflected by the substrate and collected onto a multichannel detector. **b** Optical image of the graphene flake after transfer on the SiO_2/Si substrate. The scale bar is 50 μm. **c** Scanning electron microscope image of the HS sample after the CVD growth of WS_2 on graphene, showing triangular crystals of WS_2. The scale bar is 2 μm.

interpreted as a result of an efficient interlayer charge transfer from the TMD to graphene. We can argue that in our sample the interlayer coupling is weaker and the semiconductor-to-graphene interlayer scattering channel is strongly suppressed. The weak coupling between the layers is further confirmed by photoluminescence measurements, where a small reduction of the emission quantum yield in the HS, compared to the TMD alone, is observed (see Supplementary Fig. 2).

Figure 2b reports the transient reflectivity map measured on WS_2/graphene HS for excitation below the WS_2 bandgap ($E_{pump} = 0.8$ eV). Although the pump photon energy is 1.2 eV below the optical gap of 1L-WS_2, and only the graphene layer is photoexcited, we observe a clear signature of the A/B exciton dynamics. For comparison, Fig. 2c reports the $\Delta R/R$ spectra for the pump above and below the WS_2 optical gap at $\tau = 1$ ps. Both the spectra display positive bleaching signals of the excitonic peaks and redshifted negative photoinduced absorption signals. In both the excitation regimes the ratio between the bleaching signals is almost the same, meaning that the photoexcited carriers, no matter how they are injected in the TMD layer, induce the same non-equilibrium response.

The extracted transient dynamics at the energy of the A exciton are displayed in Fig. 2d. For both the excitation conditions, the temporal traces share similar relaxation dynamics. The fast relaxation components (i.e. sub-ps and few ps) have been attributed to different processes: exciton-exciton annihilation[43], bright to dark exciton transition[44] and exciton radiative recombination[45]. Similar sub-ps relaxation dynamics have been recently observed in the same HS by time and angle-resolved photoelectron spectroscopy experiments and have been attributed to the charge-separated transient state[46]. The slow relaxation of the charge transfer signal on the order of hundreds of ps has been also reported in the transient THz photoconductivity experiments performed on large-area HSs, and it has been attributed to a detrapping process from interfacial states (i.e. defect states) forming at the interface between graphene and WS_2[30].

Interestingly, these long-lived dynamics were not observed in previous transient absorption experiments performed on small area HS prepared by mechanical exfoliation. We attribute this difference to the fact that epitaxially grown HSs display a reduced contact between the layers with respect to those formed by stacking mechanically exfoliated layers. Spatially resolved PL maps on mechanically exfoliated HSs reported μm-sized regions with good contact where the PL is strongly quenched, surrounded by other regions characterized by reduced PL quenching[26]. Our transient reflectivity and PL measurements are performed on a spatial scale on the order of 100 μm and predominantly include contributions from regions with reduced interlayer contact. A consequence of the reduced interaction is that the decay dynamics of the exciton bleaching signal are not strongly affected by the underlying graphene layer. Despite the reduced interaction, our data provide clear evidence of the directional transfer of

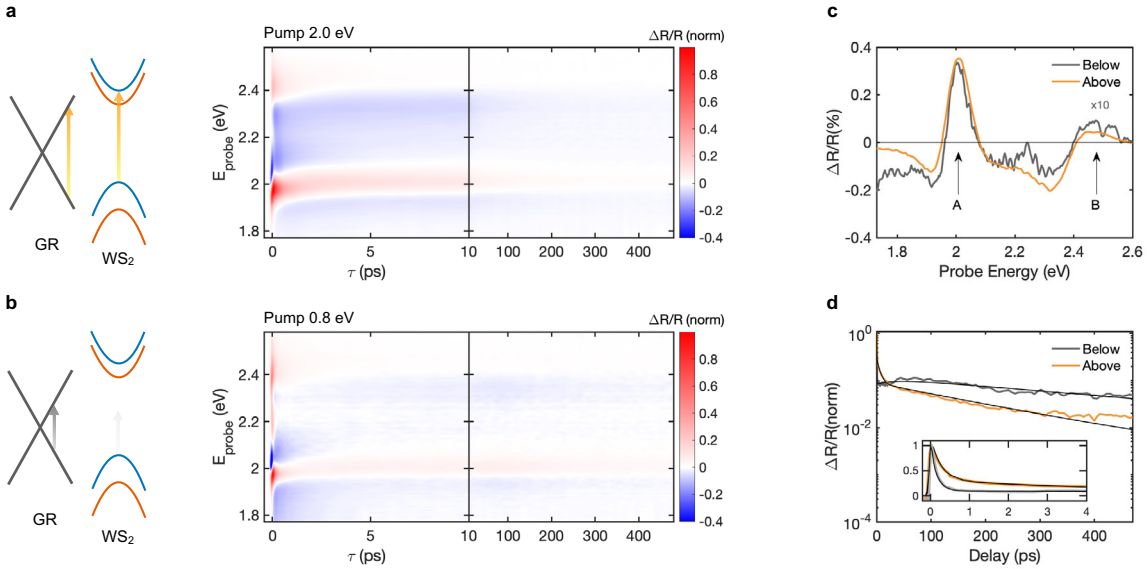

Fig. 2 Transient optical response of WS_2/graphene HS excited above and below the optical gap of 1L-WS_2. Normalized $\Delta R/R$ map of WS_2/graphene HS measured upon **a** above-gap ($E_{pump} = 2.0$ eV, fluence ~ 28 $\mu J/cm^2$) and **b** below-gap photoexcitation ($E_{pump} = 0.8$ eV, fluence ~ 61 $\mu J/cm^2$). **c** $\Delta R/R$ spectra at $\tau = 1$ ps for above (orange) and below (grey) gap excitation. In both the photoexcitation regimes $\Delta R/R$ spectra are dominated by the bleaching of the A/B excitons. **d** Normalized dynamics of the HS measured at the A excitonic resonance for both excitation regimes. In the inset a zoom in 0-4 ps delay. The black curves are the multi-exponential fits to the data. On a short timescale, for above-gap excitation (yellow), the trace decays on a timescale of $\tau_1 = 297 \pm 24$ fs and $\tau_2 = 11.9 \pm 2.3$ ps while, for below-gap excitation, $\tau_1 = 135 \pm 22$ fs and $\tau_2 = 40.5 \pm 6.4$ ps. On a longer timescale the traces display an additional slower decay component $\tau_3 = 270 \pm 196$ ps (above gap) and $\tau_3 = 704 \pm 291$ ps (below gap).

photoexcited carriers from graphene to WS_2. In fact, for below bandgap excitation, no bleaching signal is detected in isolated WS_2 (see Fig. 3a). This means that the $\Delta R/R$ signal in the HS, measured at the gap of WS_2, is originated exclusively by the fraction of the carriers photogenerated in graphene and transferred to WS_2. We exclude that the $\Delta R/R$ signal in the HS is caused by the change of the screening induced by carriers photoexcited in graphene without interlayer charge transfer. If this were the case, the transient signal in the HS would be characterized by the same relaxation time of the photoexcited carriers in graphene (i.e. few picoseconds)[7,47,48]. The long-lived (i.e. hundreds of picoseconds) relaxation component can thus only be the result of photoexcited carriers that are scattered into the WS_2 layer and are subject to the relaxation channels typical of TMDs. For the sake of completeness it is worth mentioning that heating effects[49] (related to the transient increase of the lattice temperature due to energy transfer from photoexcited carriers to the phonon system and the subsequent energy release to the substrate) might also contribute to the pump-probe signal on the long timescale. No signature of phonon recycling process[29] has been observed in the HS on the 100 ps timescale and in our used pump photon energy range.

The efficiency of the CT process, i.e. the ratio between the density of the carriers that are scattered in the WS_2 layer and the density of the carriers that are directly photoinjected in the graphene layer, is estimated to be around 15% for the excitation at ~0.8 eV (see Supplementary Note 5).

Charge transfer dynamics and hot-carrier transfer

We now focus on the physical origin of the interlayer charge transfer process. Figure 3a compares the onset of the transient dynamics at the energy of the A exciton transition as measured on WS_2/graphene, on isolated graphene and isolated WS_2, following photoexcitation by a 80 fs pulse with photon energy 0.88 eV. For the excitation fluences used in the experiment, no detectable signal is measured on isolated 1L-WS_2. This result rules out any possible multi-photon excitation process in 1L-WS_2 and unambiguously demonstrates that the $\Delta R/R$ response of the HS is determined only by the interlayer CT process from graphene. The $\Delta R/R$ signal in graphene probed at photon energies higher than the pump photon energy is strictly related to the formation of the hot-carrier distribution. The negative sign has been explained in terms of increased absorption, due to the renormalization of the bands, resulting in a change of the slopes of the Dirac cones[16]. The dashed grey line is the dynamics of graphene flipped in sign and normalized to the maximum of the HS dynamics. We measure a clear 30 fs delay in the onset of the HS dynamics (orange), compared to the dynamics of graphene, whose rise time is instantaneous, i.e. pulse-width limited (~70 fs). This result suggests that the interlayer CT process is not instantaneous as expected for a direct excitation from graphene to WS_2 electronic bands. The ~30 fs difference between the two curves gives a first direct estimation of the timescale for the transfer process.

Two different mechanisms have been proposed to account for the CT process in the graphene/1L-WS_2 HS: the direct excitation of interlayer CT transitions and the interlayer injection of hot carriers[26]. In the former process electrons are directly photoexcited from the Dirac valence band of graphene to the conduction bands of 1L-WS_2. This CT mechanism based on direct carrier excitation is not expected to take place for the pump photon energies used in the experiment. Density functional theory calculation of the HS band structure and angle-resolved photoemission measurements show that there are no possible momentum-conserving optical transitions from the valence band of graphene to the conduction band of 1L-WS_2 available for energies lower than ~1 eV[26]. In the latter process the photoexcitation creates highly non-thermal electron and hole density distributions $n(E)$ (see the photoexcitation panel in Fig. 3c), which relax into a hot-carrier distribution on a few tens of fs timescale (see the thermalization process depicted in Fig. 3c), due to ultrafast electron-electron scattering[16,17]. Within this hot

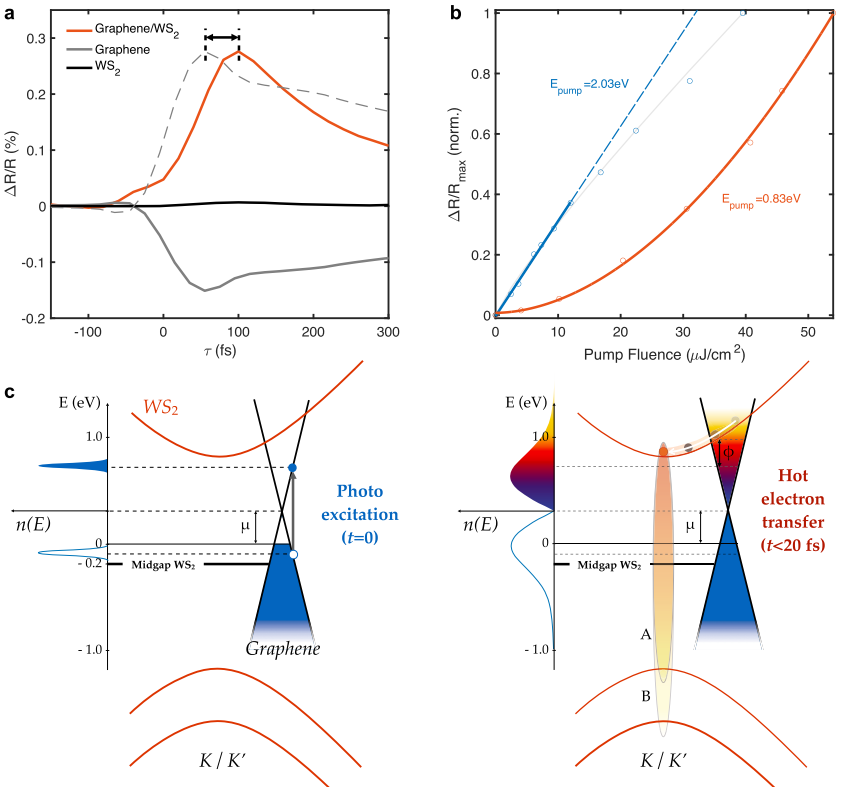

Fig. 3 Hot-electron transfer in a 1L-WS_2/graphene HS. a Onset of the transient dynamics at the A exciton energy measured on WS_2/graphene HS (orange), on isolated graphene (grey) and isolated WS_2 (black). The dashed grey line is the dynamics of graphene normalized to that of the HS. The pump photon energy is set to 0.88 eV and the fluence is ~24 $\mu J/cm^2$. The vertical lines mark the peak of the bleaching dynamics. **b** Normalized fluence dependence of the maximum of the bleaching signal ($\Delta R/R_{max}$) measured at the A exciton energy of the HS for pump excitation above (blue dots) and below (orange dots) the optical gap. The continuous lines are the fit to the data with a power-law function. $\Delta R/R_{max}$ grows linearly for above pump excitation (blue fit curve $a \sim 1$) and starts saturating above a certain fluence threeshold (25 $\mu J/cm^2$—grey fit curve $a \sim 0.9$) and non-linearly for below-gap excitation (orange fit curve—$a \approx 2$). **c** Sketch of the energy distribution of the carrier density $n(E)$[17], after photoexcitation of graphene at time delay $t = 0$, and hot-electron transfer via photothermionic process. μ is the residual doping of graphene, ϕ is the Schottky barrier, T_e and T_l are the electronic and the lattice temperature, respectively. The sketch of the band alignment follows the energy/momentum scale reported in Ref. [46].

distribution, carriers with sufficient energy to overcome the Schottky barrier ϕ can transfer to the TMD layer. Owing to the HS band alignment, it is more favourable for hot electrons rather than for hot holes to scatter from the graphene to TMD layer. In fact the energy splitting for valence band states at the K point is orders of magnitude higher (i.e. ~450 meV[32]) than the energy splitting of the conduction band states (~30 meV[50]). This results in a larger scattering phase space for hot electrons than for holes. While we cannot exclude simultaneous electron/hole transfer at the bottom/top of the conduction/valence band (A exciton bleach), it is much more likely, from the energy point of view, that the B exciton transition is bleached by photoexcited electrons in conduction band rather than holes in the valence band.

To gain further insight into the mechanism behind the CT process, we measure a fluence dependence of the $\Delta R/R$ of the HS (Fig. 3b). We find that the transient bleaching signal resulting from below-gap excitation scales super-linearly with the excitation fluence. Conversely, the transient $\Delta R/R$ signal for excitation resonant to the gap (i.e. for direct photogeneration of carriers/excitons in the TMD layer), reported as a comparison, is characterized by linear fluence dependence and saturates above a certain fluence threshold. The data are fitted with a power-law function $\Delta R/R_{max} = KF^a$ where F is the incident fluence, a is the power-law index and K is a multiplicative constant. This non-linear power dependence can only be explained in terms of a hot-carrier transfer process. In this scattering process, only the hot carriers in the high-energy tail of the non-equilibrium distribution have enough energy to overcome the Schottky barrier and to be promoted into the TMD layer. For these reasons, the power dependence of the $\Delta R/R$ signal scales non-linearly with the excitation fluence.

Hot-carrier injection timescale

Aiming to determine more precisely the timescale of the interlayer hot-electron transfer, we push the temporal resolution below 20 fs by using broadbad pump pulses at 1.2 eV photon energy compressed down to nearly transform-limited 20 fs duration[51]. Figure 4 shows the $\Delta R/R$ map measured on the HS photoexcited with this improved temporal resolution. From the map shown in Fig. 4a we can extract the transient $\Delta R/R$ dynamics of the HS at the bleaching peak of the A exciton (Fig. 4b). The data can be fitted to a function $f(t)$ given by the product of one exponential rise and one decay, i.e. $f \propto (1 - e^{-t/\tau_{rise}}) * (e^{-t/\tau_{decay}})$, convoluted by a gaussian function describing the instrumental response function, experimentally measured by the frequency-resolved optical gating technique. The extracted exponential rise time $\tau_{rise} = 12 \pm 3$ fs is comparable to the temporal resolution of our experiment. The weak negative signal observed at $t < 0$ on a broad photon energy range is related to the so-called pump-perturbed free-induction decay[52]. Since this signal occurs at negative delays and it is more that one order of magnitude smaller than the exciton bleaching

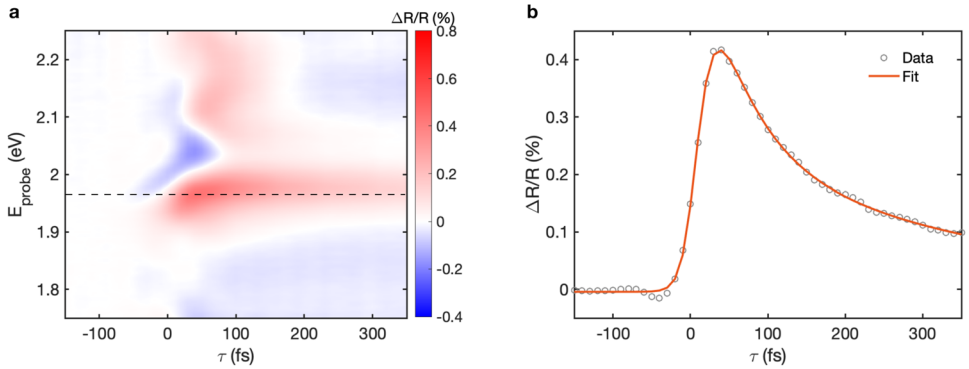

Fig. 4 Hot-carrier injection timescale. a $\Delta R/R$ map measured on the WS_2/graphene HS following a sub-20 fs excitation at 1.2 eV and **b** extracted A exciton dynamics.

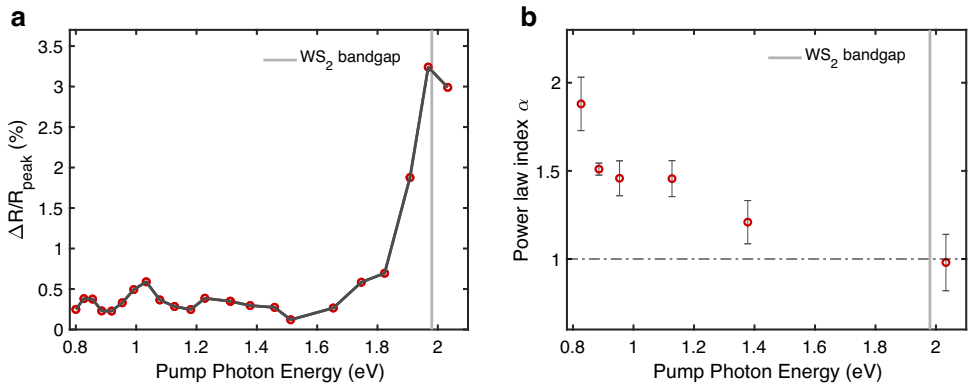

Fig. 5 Excitation photon energy dependence of the hot-carrier transfer. a Pump photon energy dependence of $\Delta R/R_{max}$ at constant incident fluence excitation ~30 $\mu J/cm^2$ measured on WS_2/graphene HS; **b** Pump photon energy dependence of the fitting parameter α, index of the power-law fitting function. Error bars represent the 95% confidence bounds of the fitted power-law indexes.

signal, it does not affect the exciton build-up dynamics and does not prevent a precise estimation of the build-up time of the WS_2 bleaching signal.

This measurement thus sets the upper limit for the hot-carrier injection time to 20 fs. We argue that this characteristic timescale found for the interlayer scattering in the HS is faster than the full electron (hole) thermalization time in graphene as calculated in Ref. [17] and comparable to the electron-electron scattering timescale. In fact, the photoexcited non-thermal carrier distribution in graphene starts thermalizing immediately after photoexcitation[7]. The transition from a non-thermal to a thermal distribution occurs within ~50 fs and its fingerprint has been reported in Ref. [7] as the change of slope of the differential transmission spectrum in single-layer graphene. The observed CT signal in our work occurs within 20 fs, meaning that hot carriers migrate from graphene to WS_2 even before the carrier thermalization is fully accomplished.

A possible reason for such a fast interlayer carrier transfer might be due to the nearly zero degree alignment between the TMD and the graphene layer of the HS. However, additional measurements of the hot-carrier scattering time on HS characterized by different controlled twist angles would be certainly beneficial for a deeper understanding of the mechanism underlying the interlayer scattering of hot carriers[53].

Pump photon energy dependence of the hot-carrier transfer process

Finally, we measure the hot-electron injection process in the HS as a function of the pump photon energy. Figure 5a reports the peak of the $\Delta R/R$ measured at the 1L-WS_2 A exciton energy upon increasing the pump energies up to the optical gap of 1L-WS_2. The amplitude of the transient signal remains almost constant in the near-IR region, as a result of the spectrally flat absorption coefficient of graphene, while it drastically increases approaching the optical gap of WS_2. The fluence dependence of $\Delta R/R_{max}$ is studied and the pump photon energy dependence of the power-law index α of the fit is reported in Fig. 5b. α rapidly decreases to unity at pump energies closer to the gap. We stress that in a few-layer WSe_2 embedded graphene the photocurrent intensity displays similar excitation photon energy dependence[27]. Similar pump photon energy dependence has been recently observed in large-area HSs by transient optical measurements performed in both the visible and the THz ranges[30]. Such a transition between two different regimes could be explained in terms of an increasing contribution of the direct excitation of the WS_2 layer as the pump photon energy approaches the gap of the TMD layer[26]. We also stress that a measurement of the graphene/TMD band alignment is necessary in order to precisely determine the energy range where hot-carrier transfer and direct excitation of CT states can coexist. Time-dependent density functional theory calculations[54] could also help to better understand the observed transition from non-linear to linear of the pump fluence dependence and to disentangle the contribution of these two processes to the pump-probe signal.

In conclusion, we have used ultrafast optical spectroscopy to visualize the ultrafast charge transfer process from graphene to WS_2 in a large-area HS excited below the semiconductor bandgap. The broad spectral coverage and the high temporal resolution of the experiment have revealed the build-up of a signal at the excitonic transition of the semiconductor on the sub-20-fs

timescale, which we assign to hot-electron transfer from graphene to 1L-WS_2. The nearly constant photoinjection rate with the excitation photon energy and the nanosecond carrier lifetime achieved in the semiconductor make this HS an ideal platform for efficient photodetection and light-harvesting applications, based on upconversion of low energy photons via hot-carrier generation and injection across a Schottky barrier. Given the availability of a large-scale growth technique for both graphene and 1L-WS_2, this HS is also promising for actual integration into large production.

METHODS

Sample preparation

Monocrystalline graphene is synthesized via CVD on electropolished copper (Cu) foils (Alfa Aesar, 99.8%) following the procedure described by Miseikis et al.[31]. The growth is performed inside a cold-wall CVD system (Aixtron BM) at a temperature of 1060 °C flowing methane, hydrogen and argon. The crystals are subsequently transferred on SiO_2/Si substrates (285 nm thick SiO_2 layer on p-doped Si, Sil'tronix) using a semi-dry procedure[31,55]. Specifically, a poly(methyl methacrylate) (PMMA AR-P 679.02 Allresist GmbH) film is used to support the graphene single crystals while detaching them from Cu using electrochemical delamination. The PMMA-coated graphene crystals are subsequently aligned with the target SiO_2/Si substrate using a micromechanical stage and finally deposited on it. WS_2 is grown directly on graphene via CVD from solid precursors, i.e. tungsten trioxide WO_3 (Sigma–Aldrich, 99.995%) and sulfur S (Sigma–Aldrich, 99.998%)[56]. The process is performed in a 2.5" horizontal hot-wall furnace (Lenton PTF). The furnace comprises a central hot-zone, where a crucible loaded with WO_3 powder was placed 20 mm away from the growth substrate, and an inlet zone, where the S powder was positioned and heated by a resistive belt, in order to separately control its temperature. S is evaporated and then carried by an argon flux to the centre of the furnace where it reacts with WO_3 directly on the sample surface at a temperature of 900 °C and at a pressure of $\sim 5 \times 10^{-2}$ mbar.

Experimental setup

We use an amplified Ti:sapphire laser (Coherent Libra), emitting 100 fs pulses at 1.55 eV, with an average power of 4 W at 2 kHz repetition rate. A 320 mW fraction of the laser power is used for our experiments. The output beam is divided by a beam splitter into pump and probe lines. We use a visible NOPA to generate ~70 fs pump pulses at tunable photon energy between 0.8 and 2 eV. The probe in the photon energy range 1.7–2.6 eV is obtained by white light continuum generation in a 1.55-eV-pumped 1 mm-thick sapphire plate, filtering out light at the fundamental frequency with a short-pass filter, and it shows rms fluctuations as low as 0.2%. For the sub-20-fs temporal resolution measurements, the pump is obtained by a near-IR NOPA[51] centered at 1.2 eV with a bandwidth of ~200 meV, while the probe in the photon energy range 1.75–2.25 eV is a sub-20-fs compressed visible NOPA. In both configurations, the reflected probe is dispersed by a grating and detected by a Si CCD camera with 532 pixels, corresponding to a bandwidth per pixel of 1.1 nm. The pump pulse is modulated at 1 kHz by a mechanical chopper, resulting in detection sensitivity of the order of 10^{-4} with an integration time of 2 s.

DATA AVAILABILITY

The data that support the plots within this paper and other findings of this study are available from the corresponding author upon reasonable request.

CODE AVAILABILITY

The code that support the data analysis of this paper are available from the corresponding author upon reasonable request.

Received: 8 January 2021; Accepted: 21 February 2022;
Published online: 28 March 2022

REFERENCES

1. Shah, J. & Iafrate, G. J. Hot Carriers in Semiconductors, 1st edn. In *Proc. Fifth International Conference*. (Pergamon, 1988).
2. Hess, K., Leburton, J. -P. & Ravaioli, U. *Hot Carriers in Semiconductors*. (Plenum Press, 1996).
3. Nozik, A. J. Spectroscopy and hot electron relaxation dynamics in semiconductor quantum wells and quantum dots. *Annu. Rev. Phys. Chem.* **52**, 193–231 (2001).
4. Shockley, W. & Queisser, H. J. Detailed balance limit of efficiency of p-n junction solar cells. *J. Appl. Phys.* **32**, 510–519 (1961).
5. Scales, C. & Berini, P. Thin-film Schottky barrier photodetector models. *IEEE J. Quantum Electron.* **46**, 633–643 (2010).
6. Lao, Y.-F. et al. Tunable hot-carrier photodetection beyond the bandgap spectral limit. *Nat. Photonics* **8**, 412–418 (2014).
7. Brida, D. et al. Ultrafast collinear scattering and carrier multiplication in graphene. *Nat. Commun.* **4**, 1987 (2013).
8. Richter, J. M. et al. Ultrafast carrier thermalization in lead iodide perovskite probed with two-dimensional electronic spectroscopy. *Nat. Commun.* **8**, 376 (2017).
9. Bonaccorso, F., Sun, Z., Hasan, T. & Ferrari, A. C. Graphene photonics and optoelectronics. *Nat. Photonics* **9**, 611–622 (2010).
10. Liu, M. et al. A graphene-based broadband optical modulator. *Nature* **474**, 64–67 (2011).
11. Liu, J. et al. Review of graphene modulators from the low to the high figure of merits. *J. Phys. D Appl. Phys.* **53**, 233002 (2020).
12. Liu, C.-H., Chang, Y.-C., Norris, T. B. & Zhong, Z. Graphene photodetectors with ultra-broadband and high responsivity at room temperature. *Nat. Nanotech.* **9**, 273–278 (2014).
13. Luo, F. et al. High responsivity graphene photodetectors from visible to near-infrared by photogating effect. *AIP Adv.* **8**, 115106 (2018).
14. Yan, H. et al. Tunable infrared plasmonic devices using graphene/insulator stacks. *Nat. Nanotech.* **7**, 330–334 (2012).
15. Grigorenko, A. N., Polini, M. & Novoselov, K. S. Graphene plasmonics. *Nat. Photonics* **6**, 749–758 (2012).
16. Breusing, M. et al. Ultrafast nonequilibrium carrier dynamics in a single graphene layer. *Phys. Rev. B* **83**, 1–4 (2011).
17. Tomadin, A., Brida, D., Cerullo, G., Ferrari, A. C. & Polini, M. Nonequilibrium dynamics of photoexcited electrons in graphene: Collinear scattering, Auger processes, and the impact of screening. *Phys. Rev. B* **88**, 035430 (2013).
18. Voisin, C. & Plaçais, B. Hot carriers in graphene. *J. Condens. Matter Phys.* **27**, 160301 (2015).
19. Voisin, C. & Plaçais, B. Energy flows in graphene: hot carrier dynamics and cooling. *J. Condens. Matter Phys.* **27**, 164201 (2015).
20. Ma, Q. et al. Tuning ultrafast electron thermalization pathways in a van der Waals heterostructure. *Nat. Phys.* **12**, 455–459 (2016).
21. Fong, K. C. et al. Measurement of the electronic thermal conductance channels and heat capacity of graphene at low temperature. *Phys. Rev. X* **3**, 41008 (2013).
22. Yu, W. J. et al. Highly efficient gate-tunable photocurrent generation in vertical heterostructures of layered materials. *Nat. Nanotech.* **8**, 952–958 (2013).
23. Bernardi, M., Palummo, M. & Grossman, J. C. Extraordinary sunlight absorption and one nanometer thick photovoltaics using two-dimensional monolayer materials. *Nano Lett.* **13**, 3664–3670 (2013).
24. Koppens, F. H. L. et al. Photodetectors based on graphene, other two-dimensional materials and hybrid systems. *Nat. Nanotech.* **9**, 780–793 (2014).
25. Massicotte, M. et al. Picosecond photoresponse in van der Waals heterostructures. *Nat. Nanotech.* **11**, 42–46 (2016).
26. Yuan, L. et al. Photocarrier generation from interlayer charge-transfer transitions in WS2-graphene heterostructures. *Sci. Adv.* **4**, 2 (2018). https://www.science.org/doi/10.1126/sciadv.1700324.
27. Massicotte, M. et al. Photo-thermionic effect in vertical graphene heterostructures. *Nat. Commun.* **7**, 12174 (2016).
28. Chen, Y., Li, Y., Zhao, Y., Zhou, H. & Zhu, H. Highly efficient hot electron harvesting from graphene before electron-hole thermalization. *Sci. Adv.* **5**, 1–8 (2019).
29. Wei, K. et al. Acoustic phonon recycling for photocarrier generation in graphene-WS2 heterostructures. *Nat. Commun.* **5**, 1–9 (2020).
30. Fu, S. et al. Long-lived charge separation following pump-wavelength-dependent ultrafast charge transfer in graphene/WS_2 heterostructures. *Sci. Adv.* **7**, eabd9061 (2021).
31. Miseikis, V. et al. Deterministic patterned growth of high-mobility large-crystal graphene: a path towards wafer scale integration. *2D Mater.* **4**, 021004 (2017).
32. Forti, S. et al. Electronic properties of single-layer tungsten disulfide on epitaxial graphene on silicon carbide. *Nat. Commun.* **9**, 1–9 (2017).
33. Rossi, A. et al. Patterned tungsten disulfide/graphene heterostructures for efficient multifunctional optoelectronic devices. *Nanoscale* **10**, 4332–4338 (2018).
34. Piccinini, G. et al. Deterministic direct growth of WS_2 on CVD graphene arrays. *2D Mater.* **7**, 014002 (2019).
35. Li, Y. et al. Measurement of the optical dielectric function of monolayer transition-metal dichalcogenides: MoS_2, $MoSe_2$, WS_2, WSe_2. *Phys. Rev. B* **90**, 205422 (2014).
36. Hill, H. M. et al. Exciton broadening in WS_2/graphene heterostructures. *Phys. Rev. B* **96**, 205401 (2017).

37. Pogna, E. A. A. et al. Photo-induced bandgap renormalization governs the ultrafast response of single-layer MoS_2. *ACS Nano* **10**, 1182–1188 (2016).
38. Cunningham, P. D., Hanbicki, A. T., McCreary, K. M. & Jonker, B. T. Photoinduced bandgap renormalization and exciton binding energy reduction in WS_2. *ACS Nano* **11**, 12601–12608 (2017).
39. Aivazian, G. et al. Many-body effects in nonlinear optical responses of 2D layered semiconductors. *2D Mater.* **4**, 025024 (2017).
40. Sie, E. J. et al. Observation of exciton redshift-blueshift crossover in monolayer WS_2. *Nano Lett.* **17**, 4210–4216 (2017).
41. He, J. et al. Electron transfer and coupling in graphene-tungsten disulfide van der Waals heterostructures. *Nat. Commun.* **5**, 5622 (2014).
42. Froehlicher, G., Lorchat, E. & Berciaud, S. Charge versus energy transfer in atomically thin graphene-transition metal dichalcogenide van der Waals heterostructures. *Phys. Rev. X* **8**, 011007 (2018).
43. Sun, D. et al. Observation of rapid exciton-exciton annihilation in monolayer molybdenum disulfide. *Nano Lett.* **14**, 5625–5629 (2014).
44. Berghäuser, G. et al. Mapping of the dark exciton landscape in transition metal dichalcogenides. *Phys. Rev. B* **98**, 020301(R) (2018).
45. Robert, C. et al. Exciton radiative lifetime in transition metal dichalcogenide monolayers. *Phys. Rev. B* **93**, 205423 (2016).
46. Aeschlimann, S. et al. Direct evidence for efficient ultrafast charge separation in epitaxial WS_2/graphene heterostructures. *Sci. Adv.* **6**, eaay0761 (2020).
47. Tielrooij, K.-J. et al. Out-of-plane heat transfer in van der Waals stacks through electron-hyperbolic phonon coupling. *Nat. Nanotech.* **13**, 41–46 (2018).
48. Ulstrup, S. et al. Ultrafast dynamics of massive dirac fermions in bilayer graphene. *Phys. Rev. Lett.* **112**, 257401 (2014).
49. Ruppert, C., Chernikov, A., Hill, H. M., Rigosi, A. F. & Heinz, T. F. The role of electronic and phononic excitation in the optical response of monolayer WS_2 after ultrafast excitation. *Nano Lett.* **17**, 644–651 (2017).
50. Kosmider, K., González, J. W. & Fernández-Rossier, J. Large spin splitting in the conduction band of transition metal dichalcogenide monolayers. *Phys. Rev. B* **88**, 245436 (2013).
51. Manzoni, C., Polli, D. & Cerullo, G. Two-color pump-probe system broadly tunable over the visible and the near infrared with sub-30fs 30 fs temporal resolution. *Rev. Sci. Instrum.* **77**, 023103 (2006).
52. Brito-Cruz, C. H., Gordon, J. P., Becker, P. C., Fork, R. L. & Shank, C. V. Dynamics of spectral hole burning. *IEEE J. Quantum Electron.* **24**, 261–269 (1988).
53. Luo, D. et al. Twist-angle-dependent ultrafast charge transfer in MoS2-graphene van der Waals heterostructures. *Nano Lett.* **21**, 8051–8057 (2021).
54. Li, L., Long, R. & Prezhdo, O. V. Charge separation and recombination in two-dimensional MoS_2/WS_2: time-domain ab initio modeling. *Chem. Mater.* **29**, 2466–2473 (2017).
55. Miseikis, V. et al. Rapid CVD growth of millimetre-sized single crystal graphene using a cold-wall reactor. *2D Mater.* **2**, 014006 (2015).
56. Rossi, A. et al. Scalable synthesis of WS_2 on graphene and h-BN: an all-2D platform for light-matter transduction. *2D Mater.* **3**, 031013 (2016).

ACKNOWLEDGEMENTS

C.T. and S.D.C. acknowledge financial support from MIUR through the PRIN 2017 Programme (Prot. 20172H2SC4). C.C. and G.C. acknowledge support by the European Union Horizon 2020 Programme under Grant Agreement No. 785219 Graphene Core 2 and Grant Agreement No. 881603 Graphene Core 3.

AUTHOR CONTRIBUTIONS

C.T. performed the ultrafast measurements. C.T., A.R., G.C. and S.D.C. conceived the experiment. G.P., S.F. and F.F. prepared and characterized the sample. C.T. and S.D.C. wrote the manuscript with the contribution of all the authors.

COMPETING INTERESTS

The authors declare no competing interests.

ADDITIONAL INFORMATION

Supplementary information The online version contains supplementary material available at https://doi.org/10.1038/s41699-022-00299-4.

Correspondence and requests for materials should be addressed to StefanoDal Conte.

Reprints and permission information is available at http://www.nature.com/reprints

Publisher's note Springer Nature remains neutral with regard to jurisdictional claims in published maps and institutional affiliations.